NANO LETTERS

Letter

pubs.acs.org/NanoLett

# An Unconventional Route to High-Efficiency Dye-Sensitized Solar Cells via Embedding Graphitic Thin Films into $TiO_2$ Nanoparticle Photoanode

Yoon Hee Jang,[†] Xukai Xin,[‡,#] Myunghwan Byun,[#] Yu Jin Jang,[†] Zhiqun Lin,[‡,#,*] and Dong Ha Kim[†,*]

[†]Department of Chemistry and Nano Science, Ewha Womans University, Seoul 120-750, Korea

[‡]School of Materials Science and Engineering, Georgia Institute of Technology, Atlanta, Georgia 30332, United States

[#]Department of Materials Science and Engineering, Iowa State University, Ames, Iowa 50011, United States

*S* *Supporting Information*

**ABSTRACT:** Graphitic thin films embedded with highly dispersed titanium dioxide ($TiO_2$) nanoparticles were incorporated for the first time into the conventional dye-sensitized solar cells (DSSCs), resulting in a remarkably improved cell efficiency due to its superior electron conductivity. Massively ordered arrays of $TiO_2$ dots embedded in carbon matrix were fabricated via UV-stabilization of polystyrene-*block*-poly(4-vinylpyridine) films containing $TiO_2$ precursors followed by direct carbonization. For dye-sensitized $TiO_2$ based solar cells containing carbon/$TiO_2$ thin layers at both sides of pristine $TiO_2$ layer, an increase of 40.6% in overall power conversion efficiency was achieved compared with neat $TiO_2$-based DSSCs. Such a remarkably improved cell efficiency was ascribed to the superior electron conductivity and extended electron lifetime elucidated by cyclic voltammetry and impedance spectroscopy.

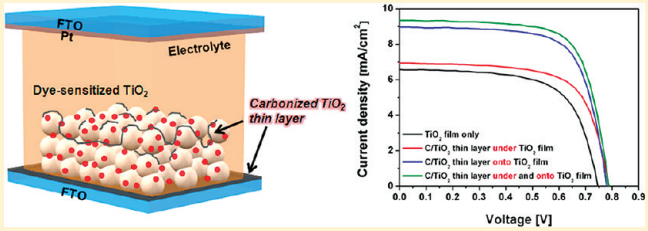


**KEYWORDS:** *Carbon/$TiO_2$ thin film, dye-sensitized solar cells, block copolymer template, direct carbonization*

Dye-sensitized solar cells (DSSCs), which are one of the most potential photovoltaic devices, have gained tremendous interest as an alternative platform to the future renewable energy production due to their high solar energy conversion efficiency as well as relatively low fabrication cost.[1−4] To date, diverse research efforts to improve the overall conversion efficiency have been intensively taken including (1) the rational design of sensitizers for increasing the light harvesting ranging from visible to near IR,[5−7] (2) optimization of semiconducting titanium dioxide ($TiO_2$) nanostructures, which strongly depends on their dimensional (e.g., size and shape) and morphological features, for facial dye loading and electron injection into the conduction band and electrode with a quantum yield of unit,[8−17] (3) the utilization of electrolytes with suitable ground- and excited-state redox potential for effective hole transport,[18,19] (4) the replacement of Pt counter electrodes with less-expensive and electrochemically stable elements,[20−24] (5) extending to a tandem cell for improving the spectral response of solar cells,[25−28] and finally (6) guarantee of long-term stability of device performance.[29,30]

Recently, unconventional approaches for enhancing solar cell performance have also been actively demonstrated. Interestingly, a dramatic increase in the charge carrier generation can be achieved by introducing novel materials such as metal nanoparticles (NPs),[31−33] periodic nanostructures,[34−36] and carbon structures into conventional solar cells. In particular, various types of carbon materials including nanotubes,[37−41] nanofibers,[42,43] and graphene[44,45] have been used to ensure high electrical conductivity, which is essential for increasing the electron collections in solar cells. Jang et al. studied that effects of incorporation of acid-treated single-wall carbon nanotubes (a-SWCNs) in $TiO_2$ film.[37] The a-SWCNs modified solar cell indicated a 25% increase in photocurrent density, which was correlated with enhanced charge transfer between the a-SWCNs and $TiO_2$ particles through the improved interconnectivity. Yang et al. introduced graphene as two-dimensional (2D) bridges into the $TiO_2$ nanostructure photoanode, which led to faster electron transport and lower recombination.[44] However, despite their potential for enabling the improved efficiency, facile, and viable strategies of coupling carbon structures into DSSCs along with plausible analysis on the operation mechanism have rarely been conducted. Therefore, big challenges still remain to clearly understand the influence on the charge collection and transport at the interface between carbon and $TiO_2$. Here we introduce a distinctly different and creative paradigm to integrate carbonized $TiO_2$ thin layers into conventional $TiO_2$ based DSSCs for improved device performance.

In our previous study, graphitic thin films with highly dispersed noble metal nanoparticles were fabricated by direct

**Received:** November 6, 2011
**Revised:** December 6, 2011
**Published:** December 12, 2011

   dx.doi.org/10.1021/nl203901m | *Nano Lett.* 2012, 12, 479−485

**Scheme 1. (a) Schematic Illustration of the Fabrication Process for Direct Carbonization of UV-Stabilized PS-*b*-P4VP/$TiO_2$ Sol-Gel Film; (b) Configuration of Solar Cells Containing Carbonized $TiO_2$ Thin Layer**

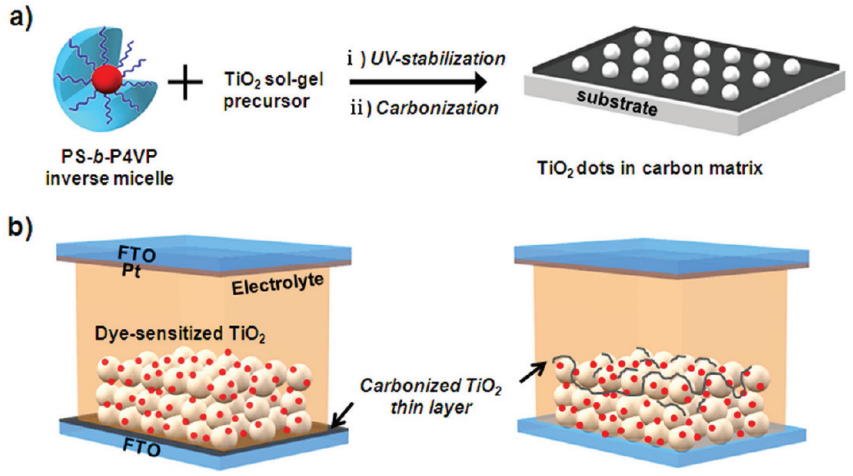


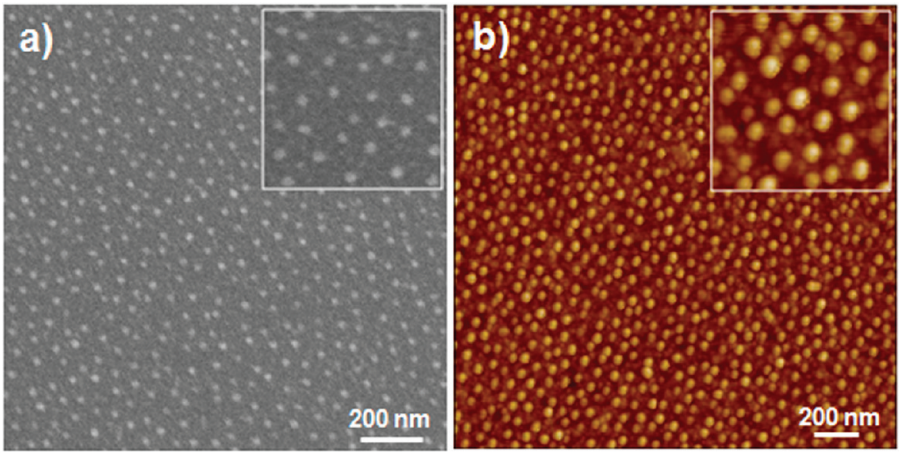


**Figure 1.** (a) SEM and (b) AFM images of $TiO_2$ dot arrays in carbon matrix. Inset images are magnified views.

carbonization of diblock copolymer (DBCP) inverse micelle templates.[46,47] Briefly, hybrid 2D metal/carbon thin films were formed by a direct carbonization of UV-cross-linked polystyrene-*block*-poly(4-vinylpyridine) (PS-*b*-P4VP) DBCPs. It is interesting to note that DBCPs can be successfully converted to carbon matrix without additional carbon sources and templates for ordered metallic NPs arrays.

On the basis of this procedure, we prepared carbonized $TiO_2$ thin layer by combining PS-*b*-P4VP DBCP self-assembly and sol−gel reactions. An appropriate amount of $TiO_2$ sol−gel precursors were added into PS-*b*-P4VP inverse micelles solution, where $TiO_2$ sol−gel precursors were selectively incorporated with P4VP blocks through the favorable coordination bonding between the titanium and the nonpair electron of nitrogen in a pyridine ring.[48] PS-*b*-P4VP/$TiO_2$ sol−gel precursor hybrid thin films were formed by spin casing, sequentially exposed to UV light and then calcined under inert condition, thus forming the ordered $TiO_2$ dot arrays in carbon matrix (more experimental details are elucidated in Experimental Methods). The overall process is schematically illustrated in the Scheme 1a. The surface morphologies of carbonized $TiO_2$ thin film were closely investigated using scanning electron microscopy (SEM) and atomic force microscopy (AFM). SEM image and corresponding height-contrast AFM image are shown in Figure 1a,b, respectively. Spatially defined arrays of $TiO_2$ dots well-distributed in carbon matrix were produced, which were retained from initial film by UV-stabilization (Supporting Information Figure S1). The average diameter, $D$, and the mean spacing between neighboring dots, $d_{c\text{-}c}$, were measured to be 15 ± 1 and 60 ± 3 nm, respectively. During the carbonization, the average value of $d_{c\text{-}c}$ was maintained, while average thickness of film was decreased about up to 80% (from 20 to 4 nm) due to volume shrinkage of DBCP. The $TiO_2$ dots are observed to be protruded from the carbon matrix film by ∼8 nm, as evaluated by the sectional profile of the AFM image in Figure 1b.

In order to investigate the nature of carbonaceous $TiO_2$, the Raman study was carried out. The Raman spectra of carbonaceous materials commonly show distinct two vibration modes, that is, the $G$ band around 1580−1600 $cm^{-1}$ and the $D$ band around 1350 $cm^{-1}$. According to a phenomenological three-stage model (amorphization trajectory) that was suggested by Ferrai and Robertson, carbonaceous materials were to be classified into three stages ranging from graphite to nanocrystalline graphite (stage 1) to amorphous carbon with maximum 20% $sp^3$ hybridized carbon atoms (stage 2) to tetrahedral amorphous carbon, the $sp^3$ content rises from ∼10−20% to ∼85% (stage 3), simply depending on the position of the $G$ band and intensity ratio of $D$ and $G$ bands.[49] The Raman spectra of neat carbon and carbon/$TiO_2$ show the characteristic


dx.doi.org/10.1021/nl203901m | *Nano Lett.* 2012, 12, 479−485

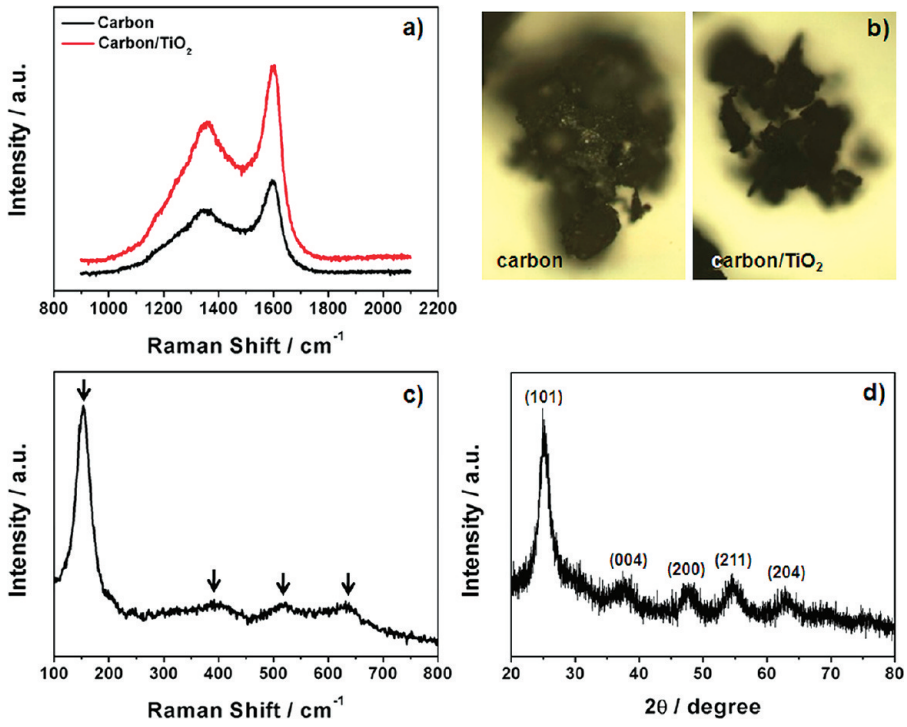


**Figure 2.** Raman spectra of (a) carbon (black) and carbonized $TiO_2$ (red) for investigating the nature of carbon. (b) Optical images of two types of powders for measuring the Raman. (c) Raman spectrum and (d) typical XRD pattern of carbonized $TiO_2$ for investigating the $TiO_2$ crystallinity.

*G* band and *D* band at about 1600 and 1350 $cm^{-1}$, respectively (Figure 2a). The shift of the *G* band position toward higher frequency indicates that PS and P4VP blocks of native PS-*b*-P4VP templates containing phenyl and pyridyl groups are successfully converted to carbon species. On the basis of the interpretation for the peak position and the ratio between the *D* and *G* band, it is reasonable to assume that carbonized products of PS-*b*-P4VP have significant portion of nanocrystalline graphitic and $sp^2$-hybridized carbon. The appearance of *D* band at lower frequency is caused by nitrogen in the pyridyl group that was acts as a defect site impeding the formation of graphitic structures.[50] Subsequently the carbonized $TiO_2$ dot arrays were crystallographycally characterized by Raman spectrum and X-ray diffraction (XRD). Figure 2c shows the Raman spectrum of carbonized $TiO_2$, which was anatase single crystal phase (arrows are characteristic modes of anatase single crystal).[51] The recorded XRD spectrum shows several characteristic peaks indexed as (101), (004), (200), (211), (204), which also correspond to typical anatase $TiO_2$ phase (JCPDS file No. 21-2172) (Figure 2d).

Carbonized $TiO_2$ thin layer would be possibly integrated into conventional DSSCs to increase the cell performance. Thin layer of carbon/$TiO_2$ dot arrays was simply introduced as under (or upper) layer (carbon/$TiO_2$ thin layer was for nothing in transparency of FTO glass, Supporting Information Figure S2) of thicker $TiO_2$ NPs film as shown in Scheme 1b. Before (or after) making the $TiO_2$ NPs film by using P25 $TiO_2$ paste,[52] thin monolayer of carbon/$TiO_2$ was formed on fluorine-doped tin oxide (FTO) substrate, and then N719 dye and iodide/triiodide redox couple were applied as sensitizer and hole transporter, respectively. Ordered $TiO_2$ dot array in carbon matrix can also be clearly seen on the rough FTO substrate, but not be observed on rough $TiO_2$ NPs film because the size of $TiO_2$ dot is not distinction from $TiO_2$ NPs (Supporting Information Figure S3). Since dropped DBCP/$TiO_2$ sol–gel solution was easily penetrated into $TiO_2$ NPs film, carbon/$TiO_2$ thin layer was expected to be interposed at the interface of $TiO_2$ NPs networks; that is another reason why carbonized $TiO_2$ dot is indistinguishable from $TiO_2$ NPs on rough $TiO_2$ NPs film.

The current–voltage (*J*–*V*) response was measured with carbonized $TiO_2$ layer incorporated $TiO_2$ NPs film electrode under frontside illumination at intensity of 100 $mW/cm^2$ and the resulting curves were plotted in Figure 3. The photoactive

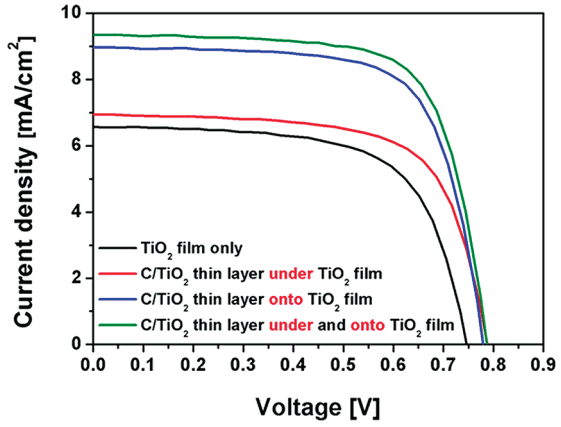


**Figure 3.** Photocurrent–voltage (*J*–*V*) characteristics of solar cells.

area for all solar cells was 0.16 $cm^2$ and thickness of $TiO_2$ NPs films was 5 $\mu$m. The corresponding results obtained from dye-sensitized $TiO_2$ solar cell with different configurations of carbon/$TiO_2$ were summarized in Table 1. Figure 3 shows the *J*–*V* characteristics for carbon/$TiO_2$ thin layer introduced into the lower (red curve), upper part (blue curve), and either side (green curve) of $TiO_2$ NPs film and only $TiO_2$ NPs film as reference electrode (black curve). The short-circuit current


dx.doi.org/10.1021/nl203901m | *Nano Lett.* 2012, 12, 479–485

**Table 1. Summary of the Photovoltaic Characteristics of DSSCs and Electrochemical Parameters Determined from EIS Analysis[a]**

| sample | $V_{oc}$ (V) | $J_{sc}$ (mA/cm$^2$) | FF | PCE (%) | $R_s$ (Ω) | $R_1$ (Ω) | $R_2$ (Ω) | $\tau_r$ (ms) |
|---|---|---|---|---|---|---|---|---|
| $TiO_2$[a] | 0.75 | 6.58 | 0.65 | 3.21 | 16.74 | 46.58 | 74.47 | 5.1 |
| lower part[b] | 0.79 | 6.94 | 0.68 | 3.71 | 16.82 | 30.00 | 64.02 | 22.1 |
| upper part[c] | 0.78 | 8.96 | 0.70 | 4.91 | 11.80 | 16.31 | 52.10 | 25.3 |
| both sides[d] | 0.79 | 9.35 | 0.71 | 5.21 | 13.39 | 18.18 | 51.84 | 29.6 |

[a]Working electrodes with different configurations: neat $TiO_2$ film; [b]carbon/$TiO_2$ thin layer introduced into lower part of $TiO_2$ film; [c]carbon/$TiO_2$ thin layer introduced into upper part of $TiO_2$ film; [d]carbon/$TiO_2$ thin layer introduced into both sides of $TiO_2$ film.

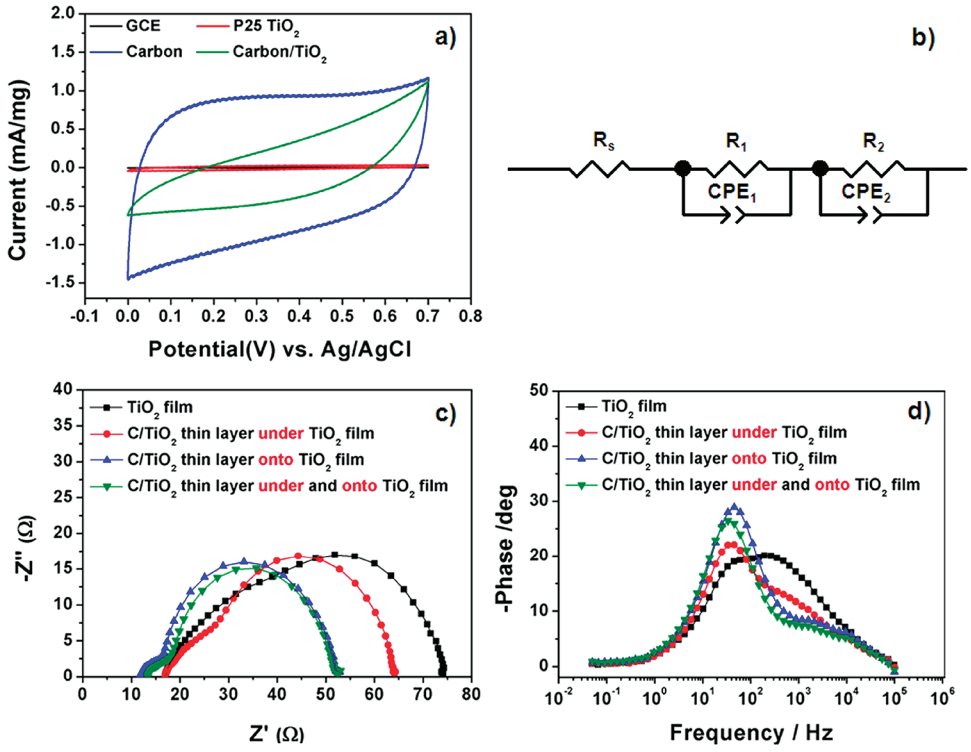


**Figure 4.** (a) Cyclic voltammetric (CV) responses for P25 $TiO_2$, carbon, and carbon/$TiO_2$ powder on glassy carbon electrode. (Scan rate: 100 mV/s). ESI data of DSSCs fabricated with four different anodes at 100 mW/cm$^2$: (b) equivalent circuit, (c) Nyquist plots, and (d) Bode phase plots. The symbols are experimental data and solid lines are the fitting results based on the equivalent circuit model.

density ($J_{sc}$) is significantly increased with the presence of thin carbonized $TiO_2$ layer and results in enhanced power conversion efficiency (PCE) compared with the reference electrode, while the values of open-circuit voltage ($V_{oc}$) and fill factor (FF) are similar with all representative samples. The values of $J_{sc}$ obtained from electrodes for carbonized $TiO_2$ thin layer introduced in the lower and upper part of $TiO_2$ NPs film are 6.94 and 8.96 mA/cm$^2$, respectively, which exhibited higher $J_{sc}$ than a $J_{sc}$ of 6.58 mA/cm$^2$ for pristine $TiO_2$ electrode. Furthermore, the highest performance, $J_{sc}$ of 9.35 mA/cm$^2$ and PCE of 5.21%, was achieved in solar cells assembled with dye-sensitized $TiO_2$ film having carbon/$TiO_2$ thin layer at both sides, which are an increase up to 40.6% from pure $TiO_2$ electrode. Higher current density depends on the amount of adsorbed dye onto the $TiO_2$ layer for DSSCs in general. Concentrations of loaded dye were calculated from UV–vis spectra of desorbed dye molecules and the value obtained from the control sample containing neat $TiO_2$ NPs was $7.19 \times 10^{-5}$ mmol/cm$^2$. In comparison, the values measured from the samples containing $TiO_2$ NPs with carbon/$TiO_2$ thin layer at lower part, upper part, and both sides were $6.09 \times 10^{-5}$, $5.78 \times 10^{-5}$, and $5.47 \times 10^{-5}$ mmol/cm$^2$, respectively (Supporting Information Figure S4). The result suggests that carbonized $TiO_2$ thin layer might partially interrupt the dye loading, leading to a decrease in the surface area for dye adsorption. And to conclude, increased photo current density is irrelevant to the dye adsorption. It is worthy to note that with the incorporation of carbonized $TiO_2$ thin layer to $TiO_2$ film, solar cell performance, particularly value of $J_{sc}$, was improved despite the slightly less amount of adsorbed dye.

In order to understand the effect of carbon/$TiO_2$ thin layer on the efficiency improvement, electron transport properties are evaluated. The electron conductivity of carbon and carbon/$TiO_2$ composites prepared by the above-described direct carbonization of DBCP inverse micelles was measured by cyclic voltammetry (CV). Figure 4a shows the typical cyclic voltammograms of carbon (blue curve), carbon/$TiO_2$ (green curve), and commercially available P25 $TiO_2$ (red curve) powders. This measurement was conducted on glassy carbon electrode (GCE) in aqueous 0.1 M KCl. The current–voltage response was maximized for pure carbon and somewhat diminished for carbon/$TiO_2$ due to the lower conductivity of $TiO_2$. Electron transport properties were investigated using electrochemical impedance spectroscopy (EIS). The internal


dx.doi.org/10.1021/nl203901m | Nano Lett. 2012, 12, 479–485

impedances determined from EIS analysis, resistance values ($R_s$, $R_1$, $R_2$) and electron recombination lifetimes ($\tau_r$) are listed in Table 1. The modeled equivalent circuit consisting of a series of resistance ($R_s$, starting point of the first semicircle in Nyquist plot), charge transport resistance at the counter electrode/electrolyte ($R_1$, first semicircle in Nyquist plot), charge transfer resistance at the photo working electrode/electrolyte ($R_2$, second semicircle in Nyquist plot), the constant phase element of capacitance corresponding to $R_1$ ($CPE_1$) and $R_2$ ($CPE_2$) was represented in Figure 4b.[53,54] In the Nyquist plots of DSSCs fabricated with four different photoanodes (Figure 4c), the internal impedances (i.e., $R_s$, $R_1$, and $R_2$) of DSSCs with carbonized thin layer were less than that of DSSCs with pure $TiO_2$ NPs film. In particular, DSSCs with carbon/$TiO_2$ thin layer at upper part (or both side) of $TiO_2$ NPs film showed the lowest total internal resistance, which is in accord with the cell performance. Electron recombination lifetime ($\tau_r$) in photoanode can be estimated from the Bode phase plots (Figure 4d). As revealed in Table 1, the presence of carbonized $TiO_2$ thin layer increases the electron lifetime and makes the electron transfer more easily. In other words, the charge transfer resistance in $TiO_2$ NPs interfaces and electron recombination are decreased, leading to a positive influence on the improvement of solar cell performance. It is thus worth noting that photogenerated charge carrier transport is facilitated through the incorporation of carbonized $TiO_2$ thin layer at two interfaces, one between carbon/$TiO_2$ and transparent conducting oxide (TCO) (i.e., FTO) and the other between $TiO_2$ NPs. It might be inferred that (1) traveling electrons are much more effectively collected to TCO via conductive carbon/$TiO_2$ thin layer and (2) conductive carbonized $TiO_2$ thin layer facilitates the electron transport at the interfaces between $TiO_2$ NPs by improving $TiO_2$ NP interconnections. In addition, further optimization of the working electrode, that is, controlling the thickness of $TiO_2$ NP layer, pre- or after treatment by $TiCl_4$, and combination of light scattering particles, is expected to lead to an improved efficiency.[55−59]

In summary, we have suggested an unconventional strategy to integrate carbonized $TiO_2$ thin layers into $TiO_2$ based conventional DSSCs for yielding improved cell efficiency. Carbonized $TiO_2$ thin layer was simply fabricated by direct carbonization of UV-stabilized DBCP scaffolds. UV-stabilization and direct carbonization ensure the successful conversion from DBCP to carbonaceous film with retaining the native structure morphology. The facial electron transfer was fulfilled when carbonized $TiO_2$ layer was inserted into $TiO_2$ film. The cell efficiencies were relatively increased up to 28.9 and 38.2% for carbon/$TiO_2$ thin layer under and onto $TiO_2$ films, respectively, than $TiO_2$ film. The $TiO_2$ film having carbon/$TiO_2$ thin layers at both sides exhibited the highest PCE of 5.21%. This was attributed to the higher electron conductivity of carbon/$TiO_2$ thin layers.

**Experimental Methods.** *Materials.* All chemicals were used as provided without further purification. Polystyrene-*block*-poly(4-vinylpyridine) diblock copolymers with polydispersity index of 1.09 was purchased from Polymer Source Inc. The number of average molecular weight of PS and P4VP were PS-*b*-P4VP, $M_n^{PS}$ = 41 kg mol$^{-1}$, $M_n^{P4VP}$ = 24 kg mol$^{-1}$, $M_w/M_n$ = 1.09, respectively. Titanium tetraisopropoxide (Ti(OCH-$(CH_3)_2)_4$, TTIP, 97%) was purchased from Sigma and acetylacetone (Acac), ethanol, hydrochloric acid (HCl), and toluene were purchased from DAE JUNG chemical and used as received.

*Preparation of Carbonized $TiO_2$ Thin Film.* PS-*b*-P4VP was dissolved in toluene and stirred at 70 °C for 2 h to yield the clear solution of inverse micelles composed of a PS corona and a P4VP core with a concentration of 0.5 wt %. Then, titanium precursor was added according to sol−gel methods.[25] Briefly, the TTIP, titanium precursor, was added to the PS-*b*-P4VP inverse micelles solution with Ti/4VP molar ratio of 4 and stirred for 24 h. Mixture of ethanol, distilled water, Acac, and HCl at a fixed molar ratio (ethanol/water/Acac/HCl = 10:10:20:0.5) was then added to polymer/titanium precursor solutions (molar ratio of titanium to Acac was adjusted to 1:4) and stirred again 24 h to completely process the sol−gel reaction. Titanium precursor was selectively incorporated into the P4VP core. In order to fabricate the PS-*b*-P4VP/titanium precursor hybrid thin film, the final common solution was spin coated on a solid substrate at 2000 rpm for 60 s. The obtained hybrid film was exposed to UV light for 1 h under vacuum condition at room temperature ($\lambda$ = 254 nm) and then subsequently carbonized in argon atmosphere by heating them to 600 °C for 1 h.

*Dye Sensitized Solar Cells with Carbonized $TiO_2$ Thin Layer Fabrication.* To fabricate DSSCs with carbonized $TiO_2$ thin layer at the lower part of $TiO_2$ NPs film, carbonized $TiO_2$ layer was fabricated on fluorine-doped tin oxide (FTO) glass substrate first. Then $TiO_2$ NPs film on carbonized $TiO_2$ layer was fabricated using homemade $TiO_2$ paste.[52] In the case where the carbon/$TiO_2$ thin layer was placed on the upper part of $TiO_2$ NPs film, the process was carried out in reverse. $TiO_2$ paste was sintered to obtain the crystalline $TiO_2$ NPs film, sensitized by the ruthenium dye (*cis*-diisothiocyanato-bis(2,2′-bipyridyl-4,4′-dicarboxylato) ruthenium(II) bis-(tetrabutylammonium), N-719, Solaronix) by immersing into 0.2 mM dye/ethanol solution for 24 h. Sputtered platinum (Pt) deposited FTO glass was used as counter electrode (average thickness of Pt is about 6.5 nm). The device was assembled by insertion of spacer (25 $\mu$m thick hot-melt sealing foil, SX1170-25, Solaronix) and an ionic liquid electrolyte (0.60 M BMIM-I, 0.03 M $I_2$, 0.50 M TBP, and 0.10 M GTC in acetonitrile/valeronitrile 85/15 (v/v) (No. ES-0004), purchased from io.li.tec, Germany) was then injected between two electrodes through the small hole of the counter electrode.

The *J*−*V* response of the DSSCs was measured under simulated AM 1.5 G illumination intensity of 100 mW/cm$^2$ using a POLARONIX K3000 Solar Cell *I*−*V* Measurement System. The photoactive area for DSSCs was 0.16 cm$^2$.

*Investigation of Electrochemical Properties.* The electron conductivity was measured at a scan rate of 100 mV/s in aqueous 0.1 M KCl electrolyte with a potentiostat (Autolab PGSTAT302N, Eco Chemie). Electrochemical impedance spectroscopy (EIS) measurements were carried out under the illumination of AM 1.5 100 mW/cm$^2$ by applying a 20 mV ac signal in the range of frequency from 50 mHz to 10 kHz with the electrochemical analyzer (IVIUMSTAT.XR, IVIUM Technologies).

*Instruments and Characterization.* The surface morphologies of prior to and after carbonization were characterized by atomic force microscopy (AFM; Dimension 3100 scanning force microscope in tapping mode (Digital Instrument)) and scanning electron microscopy (SEM; JEOL JSM6700-F). The nature of carbon and phase of $TiO_2$ were investigated by Raman spectroscopy and X-ray diffraction (XRD), respectively. Room temperature micro-Raman scattering spectra were measured using a McPherson 207 spectrometer equipped


dx.doi.org/10.1021/nl203901m | *Nano Lett.* 2012, 12, 479−485

with a nitrogen-cooled-charge-couple device array detector. The samples were excited with 488 nm line of a DPSS laser, focused to ~1 $\mu$m by using microscope objective lens (×20). The excitation laser power at the sample surfaces was estimated to be 5 mW. data were collected on a Rigaku (Dmax2000) using Ni filtered Cu K$\alpha$ radiation ($\lambda$ = 1.5418 Å). To measure the concentration of eluted dye molecules, UV−vis absorption spectroscopy (Varian Technologies/CARY 5000) was used.

## ■ ASSOCIATED CONTENT

### Supporting Information

AFM height and SEM images of PS-*b*-P4VP inverse micelle film, initial PS-*b*-P4VP/$TiO_2$ sol−gel precursor film, UV stabilized film. Optical transmittance spectra of bare FTO glass and C/$TiO_2$ thin layer on FTO glass. SEM images of bare FTO glass and $TiO_2$ NPs film. SEM images of $TiO_2$ dot array in carbon matrix on FTO glass and $TiO_2$ NPs film. UV−vis absorption spectra of eluted dye molecules from four types of photoanodes. This material is available free of charge via the Internet at http://pubs.acs.org.

## ■ AUTHOR INFORMATION

### Corresponding Author

*E-mail: (D.H.K.) dhkim@ewha.ac.kr; (Z.L.) zhiqun.lin@mse.gatech.edu.

## ■ ACKNOWLEDGMENTS

This work was supported by National Research Foundation of Korea Grant funded by the Korean Government (20110030255, 20110029409, 20110001334). This work was supported by Hi Seoul Science/Humanities Fellowship from Seoul Scholarship Foundation. Z.L. gratefully acknowledges the support from Georgia Institute of Technology.

## ■ REFERENCES

(1) O'Regan, B.; Grätzel, M. *Nature* **1991**, *353*, 737−740.
(2) Grätzel, M. *J. Photochem. Photobiol., C* **2003**, *4*, 145−153.
(3) Grätzel, M. *Inorg. Chem.* **2005**, *44*, 6841−6851.
(4) Grätzel, M. *Acc. Chem. Res.* **2009**, *42*, 1788−1798.
(5) Clifford, J. N.; Martinez-Ferrero, E.; Viterisi, A.; Palomares, E. *Chem. Soc. Rev.* **2011**, *40*, 1635−1646.
(6) Gao, F.; Wang, Y.; Shi, D.; Zhang, J.; Wang, M. K.; Jing, X. Y.; Humphry-Baker, R.; Wang, P.; Zakeeruddin, S. M.; Gratzel, M. *J. Am. Chem. Soc.* **2008**, *130*, 10720−10728.
(7) Shankar, K.; Bandara, J.; Paulose, M.; Wietasch, H.; Varghese, O. K.; Mor, G. K.; LaTempa, T. J.; Thelakkat, M.; Grimes, C. A. *Nano Lett.* **2008**, *8*, 1654−1659.
(8) Goh, C.; Coakley, K. M.; McGehee, M. D. *Nano Lett.* **2005**, *5*, 1545−1549.
(9) Haque, S. A.; Handa, S.; Peter, K.; Palomares, E.; Thelakkat, M.; Durrant, J. R. *Angew. Chem., Int. Ed.* **2005**, *44*, 5740−5744.
(10) Mor, G. K.; Shankar, K.; Paulose, M.; Varghese, O. K.; Grimes, C. A. *Nano Lett.* **2006**, *6*, 215−218.
(11) Tan, B.; Wu, Y. Y. *J. Phys. Chem. B* **2006**, *110*, 15932−15938.
(12) Koo, H. J.; Kim, Y. J.; Lee, Y. H.; Lee, W. I.; Kim, K.; Park, N. G. *Adv. Mater.* **2008**, *20*, 195−199.
(13) Wang, J.; Lin, Z. *Chem. Mater.* **2008**, *20*, 1257−1261.
(14) Wang, J.; Lin, Z. *J. Phys. Chem. C* **2009**, *113*, 4026−4030.
(15) Wang, J.; Zhao, L.; Lin, V. S. Y.; Lin, Z. *J. Mater. Chem.* **2009**, *19*, 3682−3687.
(16) Wang, J.; Lin, Z. *Chem. Mater.* **2010**, *22*, 579−584.
(17) Ye, M.; Xin, X.; Lin, C.; Lin, Z. *Nano Lett.* **2011**, *11*, 3214−3220.
(18) Nakade, S.; Kanzaki, T.; Wada, Y.; Yanagida, S. *Langmuir* **2005**, *21*, 10803−10807.
(19) Yanagida, S.; Yu, Y. H.; Manseki, K. *Acc. Chem. Res.* **2009**, *42*, 1827−1838.
(20) He, J. J.; Lindstrom, H.; Hagfeldt, A.; Lindquist, S. E. *J. Phys. Chem. B* **1999**, *103*, 8940−8943.
(21) Imoto, K.; Takahashi, K.; Yamaguchi, T.; Komura, T.; Nakamura, J.; Murata, K. *Sol. Energy Mat. Sol. Cells* **2003**, *79*, 459−469.
(22) Murakami, T. N.; Ito, S.; Wang, Q.; Nazeeruddin, M. K.; Bessho, T.; Cesar, I.; Liska, P.; Humphry-Baker, R.; Comte, P.; Pechy, P.; Gratzel, M. *J. Electrochem. Soc.* **2006**, *153*, A2255−A2261.
(23) Lin, C. Y.; Lin, J. Y.; Wan, C. C.; Wei, T. C. *Electrochim. Acta* **2011**, *56*, 1941−1946.
(24) Xin, X.; He, M.; Han, W.; Jung, J.; Lin, Z. *Angew. Chem., Int. Ed.* **2011**, *50*, 11739−11742.
(25) He, J. J.; Lindstrom, H.; Hagfeldt, A.; Lindquist, S. E. *Sol. Energy Mat. Sol. Cells* **2000**, *62*, 265−273.
(26) Durr, M.; Bamedi, A.; Yasuda, A.; Nelles, G. *Appl. Phys. Lett.* **2004**, *84*, 3397−3399.
(27) Kubo, W.; Sakamoto, A.; Kitamura, T.; Wada, Y.; Yanagida, S. *J. Photochem. Photobiol., A.* **2004**, *164*, 33−39.
(28) Nattestad, A.; Mozer, A. J.; Fischer, M. K. R.; Cheng, Y. B.; Mishra, A.; Bauerle, P.; Bach, U. *Nat. Mater.* **2010**, *9*, 31−35.
(29) Hinsch, A.; Kroon, J. M.; Kern, R.; Uhlendorf, I.; Holzbock, J.; Meyer, A.; Ferber, J. *Prog. Photovoltaics* **2001**, *9*, 425−438.
(30) Hara, K.; Wang, Z. S.; Cui, Y.; Furube, A.; Koumura, N. *Energy Environ. Sci.* **2009**, *2*, 1109−1114.
(31) Standridge, S. D.; Schatz, G. C.; Hupp, J. T. *J. Am. Chem. Soc.* **2009**, *131*, 8407−8409.
(32) Atwater, H. A.; Polman, A. *Nat. Mater.* **2010**, *9*, 205−213.
(33) Brown, M. D.; Suteewong, T.; Kumar, R. S. S.; D'Innocenzo, V.; Petrozza, A.; Lee, M. M.; Wiesner, U.; Snaith, H. J. *Nano Lett.* **2011**, *11*, 438−445.
(34) Guldin, S.; Huttner, S.; Kolle, M.; Welland, M. E.; Muller-Buschbaum, P.; Friend, R. H.; Steiner, U.; Tetreault, N. *Nano Lett.* **2010**, *10*, 2303−2309.
(35) Colodrero, S.; Mihi, A.; Haggman, L.; Ocana, M.; Boschloo, G.; Hagfeldt, A.; Miguez, H. *Adv. Mater.* **2009**, *21*, 764−770.
(36) Lee, B.; Hwang, D. K.; Guo, P. J.; Ho, S. T.; Buchholtz, D. B.; Wang, C. Y.; Chang, R. P. H. *J. Phys. Chem. B* **2010**, *114*, 14582−14591.
(37) Jang, S. R.; Vittal, R.; Kim, K. J. *Langmuir* **2004**, *20*, 9807−9810.
(38) Lee, T. Y.; Alegaonkar, P. S.; Yoo, J. B. *Thin Solid Films* **2007**, *515*, 5131−5135.
(39) Yen, C. Y.; Lin, Y. F.; Liao, S. H.; Weng, C. C.; Huang, C. C.; Hsiao, Y. H.; Ma, C. C. M.; Chang, M. C.; Shao, H.; Tsai, M. C.; Hsieh, C. K.; Tsai, C. H.; Weng, F. B. *Nanotechnology* **2008**, *19*, 375305.
(40) Umeyama, T.; Imahori, H. *Energy Environ. Sci.* **2008**, *1*, 120−133.
(41) Dang, X. N.; Yi, H. J.; Ham, M. H.; Qi, J. F.; Yun, D. S.; Ladewski, R.; Strano, M. S.; Hammond, P. T.; Belcher, A. M. *Nat. Nanotechnol.* **2011**, *6*, 377−384.
(42) Liu, J. W.; Kuo, Y. T.; Klabunde, K. J.; Rochford, C.; Wu, J.; Li, J. *ACS Appl. Mater. Inter* **2009**, *1*, 1645−1649.
(43) Rochford, C.; Li, Z. Z.; Baca, J.; Liu, J. W.; Li, J.; Wu, J. *Appl. Phys. Lett.* **2010**, 97.
(44) Yang, N.; Zhai, J.; Wang, D.; Chen, Y.; Jiang, L. *ACS Nano* **2010**, *4*, 887−894.
(45) Sun, S. R.; Gao, L.; Liu, Y. Q. *Appl. Phys. Lett.* **2010**, 96.
(46) Wang, Y.; Liu, J. Q.; Christiansen, S.; Kim, D. H.; Goesele, U.; Steinhart, M. *Nano Lett.* **2008**, *8*, 3993−3997.
(47) Jang, Y. H.; Kochuveedu, S. T.; Jang, Y. J.; Shin, H. Y.; Yoon, S.; Steinhart, M.; Kim, D. H. *Carbon* **2011**, *49*, 2120−2126.
(48) Song, L. X.; Lam, Y. M.; Boothroyd, C.; Teo, P. W. *Nanotechnology* **2007**, *18*, 135605.
(49) Ferrari, A. C.; Robertson, J. *Phys. Rev. B* **2000**, *61*, 14095−14107.
(50) Ferrari, A. C.; Rodil, S. E.; Robertson, J. *Phys. Rev. B* **2003**, *67*, 155306.

(51) Ohsaka, T.; Izumi, F.; Fujiki, Y. *J. Raman Spectrosc.* **1978**, *7*, 321−324.
(52) Ito, S.; Chen, P.; Comte, P.; Nazeeruddin, M. K.; Liska, P.; Péchy, P.; Grätzel, M. *Prog. Photovotaics* **2007**, *15*, 603−612.
(53) Han, L. Y.; Koide, N.; Chiba, Y.; Mitate, T. *Appl. Phys. Lett.* **2004**, *84*, 2433−2435.
(54) Koide, N.; Islam, A.; Chiba, Y.; Han, L. Y. *J. Photochem. Photobiol., A* **2006**, *182*, 296−305.
(55) Wang, Z. S.; Kawauchi, H.; Kashima, T.; Arakawa, H. *Coord. Chem. Rev.* **2004**, *248*, 1381−1389.
(56) Hou, K.; Tian, B. Z.; Li, F. Y.; Bian, Z. Q.; Zhao, D. Y.; Huang, C. H. *J. Mater. Chem.* **2005**, *15*, 2414−2420.
(57) Ito, S.; Zakeeruddin, S. M.; Humphry-Baker, R.; Liska, P.; Charvet, R.; Comte, P.; Nazeeruddin, M. K.; Péchy, P.; Takata, M.; Miura, H.; Uchida, S.; Grätzel, M. *Adv. Mater.* **2006**, *18*, 1202−1205.
(58) Ito, S.; Murakami, T. N.; Comte, P.; Liska, P.; Grätzel, C.; Nazeeruddin, M. K.; Grätzel, M. *Thin Solid Films* **2008**, *516*, 4613−4619.
(59) Xin, X.; Scheiner, M.; Ye, M.; Lin, Z. *Langmuir* **2011**, *27*, 14594−14598.